

# Bathymetric Mapping of Shallow Water in Thaw Lakes on the North Slope of Alaska with Spaceborne Imaging Radar

NICKOLAI KOZLENKO<sup>1,2</sup> and MARTIN O. JEFFRIES<sup>1</sup>

(Received 18 July 1999; accepted in revised form 12 April 2000)

**ABSTRACT.** Few bathymetric maps are available for the thousands of thaw lakes on the North Slope of Alaska. We describe a semiautomated procedure for bathymetric mapping of water up to 2 m deep (i.e., less deep than the maximum ice thickness) in these lakes. A sequence of ERS-1 synthetic aperture radar (SAR) images and a simulated ice growth curve for winter 1991–92 are used to derive a digital elevation model of lake basins. The method is based on discriminating between floating ice and grounded ice in the SAR images to define raw isobaths; assigning an ice thickness or water depth to each isobath from the simulated ice-growth curve, and interpolating to create equally spaced (0.25 m) isobaths. There is modest agreement between SAR-derived maps and the few available bathymetric maps. Differences between the SAR maps and the original maps are probably unavoidable because of different production methods and original data formats. The concept of using SAR and a simulated ice-growth curve for bathymetric mapping of thaw lakes would benefit from verification based on a comparison with new maps derived from accurate field measurements at a selection of lakes with different morphological characteristics. Nevertheless, it is concluded that this technique is sound and could be used routinely for inexpensive and accurate bathymetric mapping across the entire North Slope and elsewhere (e.g., in Siberia, where large numbers of thaw lakes also occur). Such mapping would greatly increase the amount and spatial coverage of bathymetric data and would provide an accurate baseline against which to detect changes in the size, shape, bottom topography, and location of lakes.

**Key words:** thaw lakes, lake ice, synthetic aperture radar, bathymetric mapping, simulated ice growth, SAR-backscatter, digital elevation model

**RÉSUMÉ.** Peu de cartes bathymétriques sont disponibles pour les milliers de lacs thermokarstiques situés sur le versant Nord de l'Alaska. On décrit une procédure semi-automatisée pour la cartographie bathymétrique de l'eau jusqu'à une profondeur de 2 m (c.-à-d., inférieure à l'épaisseur maximale de la glace) dans ces lacs. On utilise une séquence d'images prises au radar à antenne synthétique (SAR) ERS-1 ainsi qu'une courbe simulée de croissance de la glace pour l'hiver 1991–1992 afin d'obtenir un modèle numérique d'altitude des bassins lacustres. La méthode est fondée sur la discrimination entre la glace flottante et la glace échouée, sur les images SAR, en vue de définir des isobathes brutes; sur l'attribution d'une épaisseur de glace ou d'une profondeur d'eau à chaque isobathe obtenue à partir de la courbe simulée de croissance de la glace, et sur l'interpolation visant à créer des isobathes équidistantes (0,25 m). Il existe une légère concordance entre les cartes issues du SAR et les quelques cartes bathymétriques disponibles. Des différences entre les cartes SAR et les cartes originales sont probablement inévitables en raison de la diversité des méthodes de production et du format des données originales. L'idée d'utiliser le SAR et une courbe simulée de croissance de la glace pour la cartographie bathymétrique des lacs thermokarstiques tirerait profit d'une vérification fondée sur une comparaison avec de nouvelles cartes issues de mesures précises effectuées sur le terrain à des lacs choisis pour leurs différentes caractéristiques morphologiques. On conclut néanmoins que c'est une bonne technique qui pourrait être utilisée couramment pour la cartographie bathymétrique économique et précise de l'ensemble du versant Nord et d'ailleurs (p. ex., en Sibérie, où l'on trouve nombre de lacs thermokarstiques). Une telle cartographie augmenterait de beaucoup la quantité et la couverture spatiale des données bathymétriques et offrirait une référence précise par rapport à laquelle il serait possible de détecter les changements dans la taille, la forme, la topographie du fond des lacs ainsi que leur emplacement.

**Mots clés:** lacs thermokarstiques, glace lacustre, radar à antenne synthétique, cartographie bathymétrique, croissance simulée de la glace, rétrodiffusion SAR, modèle numérique d'altitude

Traduit pour la revue *Arctic* par Nésida Loyer.

## INTRODUCTION

Shallow thaw lakes are a characteristic feature of the tundra landscape of the North Slope of Alaska (hereafter

referred to as the North Slope). There are thousands of lakes, as the radar image in Figure 1 shows, and in some locations they cover as much as 40% of the surface area (Sellmann et al., 1975a). The presence of continuous

<sup>1</sup> Geophysical Institute, University of Alaska, 903 Koyukuk Drive, P.O. Box 757320, Fairbanks, Alaska 99775-7320, U.S.A.

<sup>2</sup> Corresponding author: kozlenko@sf.alaska.edu

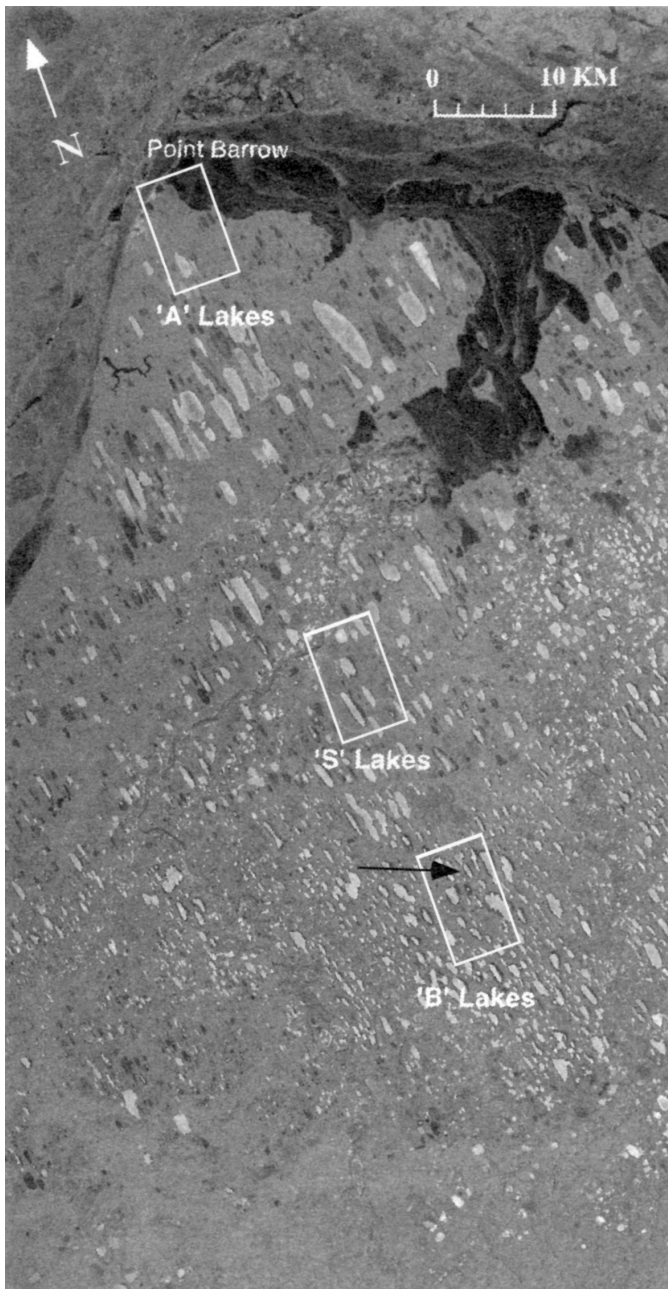


FIG. 1. Radiometrically corrected, geocoded, low resolution ERS-2 SAR image of the Barrow region of northwestern Alaska on 9 April 1997. The many elongated bright features are those areas of lakes where the ice is afloat. The location of the 'A' Lakes, 'B' Lakes and 'S' Lakes regions where existing lake bathymetry data are available, and where we derived lake bathymetry data using SAR, are identified. The arrow identifies the location of Lake B1. The original SAR image is © ESA.

permafrost in the region prohibits water from percolating into the ground, resulting in extensive wetlands with numerous lakes and ponds (Dean and Morrissey, 1988). The lakes and ponds are thought to migrate slowly, and they are known to drain rapidly; consequently, they are the primary mechanism of regional landscape modification (Sellmann et al., 1975a). The lakes and ponds have a significant impact on the ground thermal regime. Below lakes more than 2 m deep, the permafrost thaws, and perennial thaw

bulbs (taliks) form; below lakes less than 2 m deep, only thin, seasonally thawing and freezing zones occur (Brewer, 1958; Lachenbruch et al., 1962). In winter, the heat flow from the lakes to the atmosphere is on a par with that of the nearby Arctic Ocean (Jeffries et al., 1999). The lakes contribute a significant quantity of methane to the atmosphere when the ice melts in the spring (Phelps et al., 1998). They are a valuable natural resource, providing vital habitat for wildlife and aquatic fauna and water for public and industrial use (Mellor, 1982, 1994). To manage water resources to meet user demands, and to understand the role of the lakes in atmosphere–ice–land interactions, knowledge of water depth and availability are needed. Few such data are currently available.

Because the water depth in parts of all the lakes, and sometimes the entire area of many other lakes, is less than the maximum ice thickness, large areas of ice freeze completely to the bottom each winter. Since the 1970s, it has been known that the floating and grounded ice (frozen to the bottom) can be differentiated from each other in radar images (Sellmann et al., 1975b; Weeks et al., 1977, 1978, 1981). Mellor (1982) exploited this difference to create a bathymetric map of a lake using a sequence of analogue (hard copy) airborne radar images and concurrent ice thickness measurements. Mellor (1994) subsequently looked at the same lake in digital ERS-1 spaceborne synthetic aperture radar (SAR) images and found a close correspondence between the floating and grounded ice areas in the ERS-1 data and those originally identified in the airborne radar images.

Mellor (1982) pioneered the use of imaging radar for bathymetric mapping of the thaw lakes, but routine implementation would have been difficult and expensive if it continued to depend on (a) analogue images and (b) ice thickness data obtained by direct measurements on the ground. This problem was initially addressed by Jeffries et al. (1996), who used a winter-long sequence of digital ERS-1 SAR images of the Barrow region of northwest Alaska (Fig. 1) to identify the number of lakes that had frozen completely to the bottom, and a simulated ice-growth curve to estimate the maximum depth of those lakes. In this sequel to Jeffries et al. (1996), we describe a semiautomated procedure to map the bathymetry of the shallow water ( $\leq 2$  m) in thaw lakes based on the extraction of the boundaries between floating ice and grounded ice in a sequence of digital ERS-1 SAR images.

#### SAR SIGNATURES OF FLOATING AND GROUNDED LAKE ICE

This section reviews the physical basis for the contrasting SAR signatures of floating and grounded ice, since the extraction of the boundary between them is the key to the bathymetric mapping procedure.

Early remote sensing studies of the North Slope in late winter used airborne X-band real aperture radar (9.4 GHz

frequency, 32 mm wavelength) and L-band SAR (1.2 GHz frequency, 250 mm wavelength). These studies revealed a significant difference in radar backscatter intensity between the outer and inner portions of thaw lakes, which were characterized by dark and light tones, respectively (Sellmann et al., 1975b; Elachi et al., 1976; Weeks et al., 1977, 1978). These tonal differences are illustrated in Figure 2, which shows an increase in the area of dark tones as the winter progresses. It was hypothesized that the dark tones (low backscatter intensity) represented areas of grounded ice and the light tones (high backscatter intensity) represented areas of floating ice (Sellmann et al., 1975b; Weeks et al., 1977, 1978). This hypothesis has been confirmed by field measurements (Weeks et al., 1981; Jeffries et al., 1994) and numerical modeling (Wakabayashi et al., 1994).

Figure 3 is a conceptual diagram of the “double-bounce” backscatter model that explains the contrasting backscatter signatures of floating and grounded ice. At imaging radar frequencies, dry snow has a very high penetration depth and is “transparent” to the radar signal (Hallikainen and Winebrenner, 1992), which passes through to the underlying lake ice. The ice too has a high radar penetration depth (Hallikainen and Winebrenner, 1992), and the signal passes through to the ice/water interface, reflecting off vertically oriented, tubular bubbles on its way there (Fig. 3). This is the double bounce, which results in the return of a significant part of the incident energy to the satellite at nearly the same angle as it was initially transmitted (Weeks et al., 1978; Mellor, 1982; Wakabayashi et al., 1994). Consequently, floating ice with tubular bubbles causes strong backscatter and appears bright in radar images (Figs. 1 and 2).

Vertically oriented tubular bubbles also occur in grounded ice (Weeks et al., 1978, 1981; Jeffries et al., 1994), but their impact is negligible beyond serving to direct the signal to the ice/frozen soil interface. There, because of the low dielectric contrast between ice and frozen soil, the signal passes into the soil, where it is absorbed (Fig. 3). Consequently, there is minimal backscatter, and grounded ice appears dark in radar images (Weeks et al., 1978; Mellor, 1982; Wakabayashi et al., 1994). Thus, in Figure 2, the increase in the area of dark tones as the winter progresses is due to the increase in the area of ice that has frozen to the bottom. In one case, the entire lake froze to the bottom.

Mellor (1982, 1994) showed that backscatter from floating ice varies according to the density of tubular bubbles in the ice. Jeffries et al. (1996: Fig. 7) illustrated the subtle backscatter (grey scale) difference between ice floating on water that is 2–4 m deep and ice floating on water more than 4 m deep. Mellor (1982, 1994) used this backscatter variability to manually draw the 4 m isobath in lake depth maps. We were unsuccessful in our attempts to map the 4 m isobath unambiguously using the semiautomated procedure to be described in this paper. This was because the backscatter difference between these two “types” of floating ice is much smaller than that between any floating ice

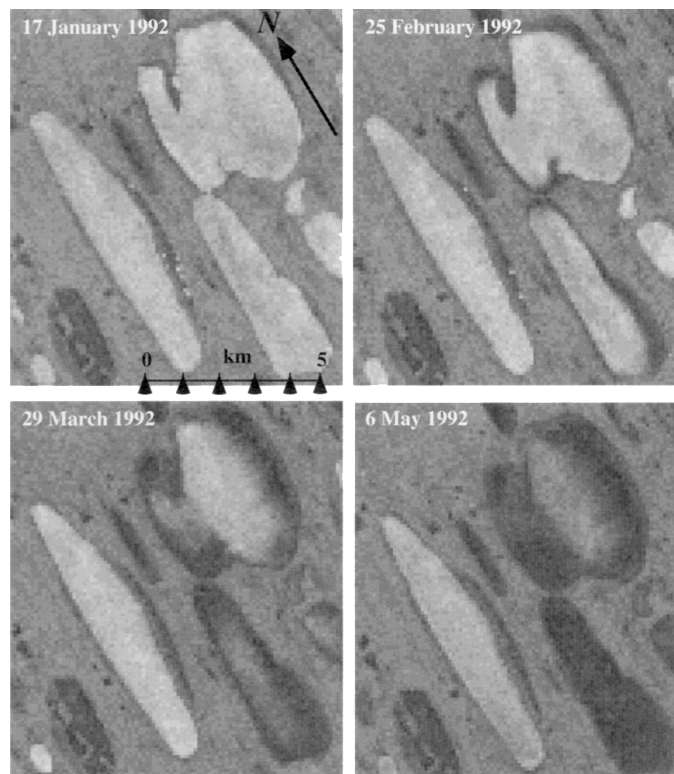


FIG. 2. ERS-1 SAR subscenes of lakes near Barrow illustrate spatial and temporal changes in tone (backscatter intensity) due to the progressive freezing of ice to the bottom of the lakes (source: Jeffries et al., 1996). The original SAR images are © ESA.

and grounded ice, and the boundaries between the two floating ice types are much more diffuse than those between any floating ice and grounded ice. Consequently, we derive isobaths only for water with depths of 2 m or less.

## LAKE BATHYMETRY MAPPING

### *Description of SAR Data*

Full-resolution ERS-1 SAR images (4-look, 30 m spatial resolution, 12.5 m pixel size) were obtained from the Alaska SAR Facility (ASF). The ERS-1 SAR is a C-band (5.3 GHz frequency, 57 mm wavelength) VV-polarization instrument. The SAR data were radiometrically calibrated and geocoded using software available from ASF. The reader is referred to the ASF Home Page (<http://www.asf.alaska.edu>) on the World Wide Web for details of the SAR instrument, product specifications, and data-processing algorithms. Thirteen images covering the interval 9 December 1991 to 29 March 1992 were used to determine lake bathymetry.

Images acquired before 9 December could not be used because of low backscatter contrast between floating and grounded ice. This phenomenon was not unique to autumn 1991. We have observed it in autumn SAR data every year that ERS-1 and ERS-2 (launched in 1995 with a SAR instrument identical to ERS-1) have been in operation.

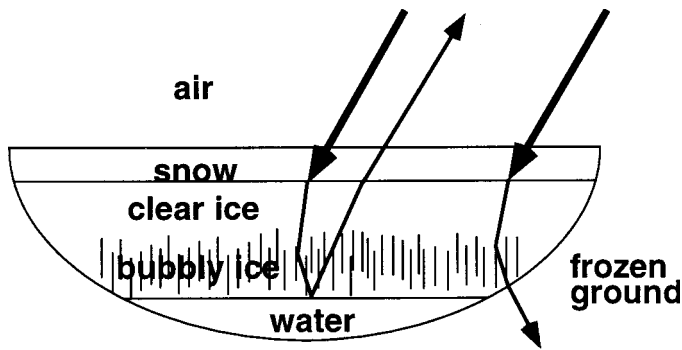


FIG. 3. Conceptual diagram of radar scattering from floating and grounded ice on shallow, thaw lakes.

Low contrast between the areas of floating and grounded ice in the early autumn images is most likely due to the fact that the lake ice is almost clear in that season. Thus it lacks the tubular bubbles (Jeffries et al., 1994) necessary for the “double bounce” that leads to strong backscatter from floating ice. The tubular bubbles begin to form only when the lake water has become supersaturated with gases, which typically occurs in late autumn (Jeffries et al., 1994).

We use Lake B1 in the ‘B’ Lakes region (Fig. 1) to illustrate the procedure for bottom mapping and production of a bathymetric chart. “B1” is the original designation of Mellor (1982). Figure 4 shows a sequence of six ERS-1 SAR subscenes of Lake B1; these are a subset of the thirteen images acquired from December 1991 to March 1992. Both the strong backscatter (bright tone) from the floating ice and the weak backscatter (dark tone) from the grounded ice are evident, and the boundary between floating and grounded ice is clearly defined. Particularly strong backscatter is evident as bright, narrow bands along some edges of the floating ice on 14 January, 2 March, and 29 March (Fig. 4). This strong backscatter is probably due to a higher density of tubular bubbles that formed as the ice was growing from shallow waters, which can have local dissolved gas concentrations higher than those in the deeper waters farther offshore (Mellor, 1982). As the winter progresses and ice thickness increases, the area of floating ice decreases as more ice freezes to the bottom. The boundary between grounded ice and tundra is also clearly defined, because the dielectric properties of tundra soils and vegetation and their influence on scattering differ from those of both the grounded and floating ice (Morrissey et al., 1996).

Backscatter from the floating ice is noticeably lower on 20 March than on 2 March and 29 March, but there are no significant differences in backscatter from the grounded ice and tundra on those dates (Fig. 4). We cannot explain this. Under the right circumstances, a decrease in backscatter from ice can be caused by an increase in snow wetness due to melting (Hallikainen and Winebrenner, 1992). However, this explanation does not apply here because backscatter did not decrease across the entire SAR scene and the maximum temperatures at Barrow on 19 and

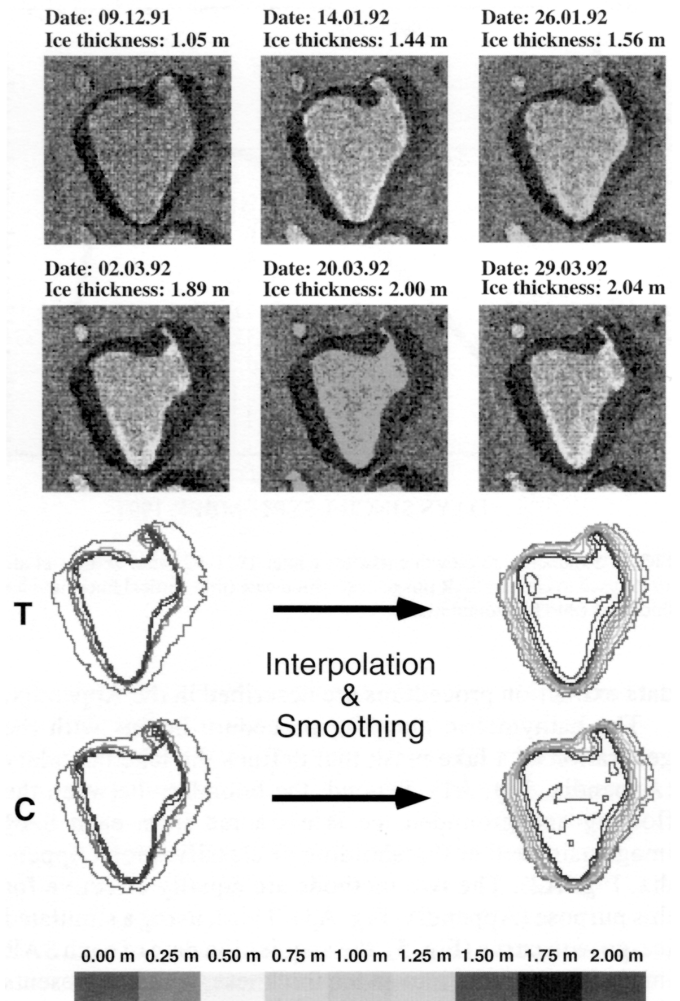


FIG. 4. This sequence of six radiometrically calibrated SAR subscenes of Lake B1 illustrates that the floating ice (light tone) is ringed by an increasing area of grounded ice (dark tone) as the winter progresses and the ice thickness increases. Above each image are the SAR data acquisition date and the ice thickness at the boundary between the floating and grounded ice on that date, as determined from the simulated ice growth curve (Fig. 5). Maps labelled T and C at lower left show the boundaries between floating and grounded ice extracted from each subscene using thresholding (T) and classification (C). The maps at lower right are the result of using interpolation and smoothing of those boundaries (raw isobaths) to create regularly spaced isobaths. The bathymetry legend of water depths at the bottom applies only to the two bathymetric maps at lower right.

20 March were  $-18.3^{\circ}\text{C}$  and  $-15.5^{\circ}\text{C}$ , respectively (NOAA, 1992). Flooding of the snow/ice interface can increase wetness at the base of the snow cover. However, this is an unlikely explanation for the decrease in backscatter on 20 March, since flooding on Antarctic sea ice and refreezing of the flooded layer on lake ice both cause an increase, not a decrease, in backscatter (Lytle et al., 1996; Leconte and Klassen, 1991).

#### Bathymetric Mapping Procedure

A condensed, general description of the bathymetric mapping procedure is provided here. The full technical details of the semiautomated SAR image processing and

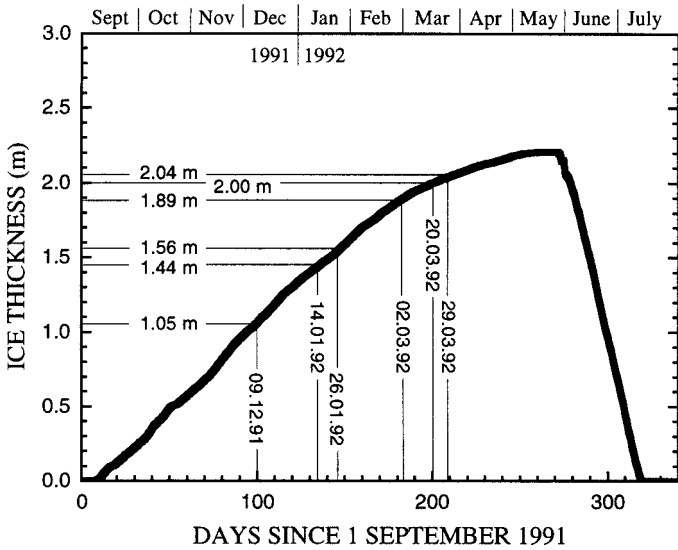


FIG. 5. Simulated ice growth curve for winter 1991–92 (after Jeffries et al., 1996) used to convert SAR image acquisition date (thin vertical lines) into ice thickness (thin horizontal lines).

data extraction procedures are described in the Appendix.

The bathymetric mapping procedure begins with the generation of a lake mask that defines the lake boundary (Appendix, Fig. A1). Second, the boundary between the floating and grounded ice is extracted from each SAR image using either thresholding or classification (Appendix, Fig. A2). The two methods are equally effective for this purpose (Appendix, Fig. A3). Third, using a simulated ice-growth curve (Fig. 5), the acquisition date of each SAR image is converted into an ice thickness, which represents the water depth at the boundary between the floating and grounded ice in each image. The extracted boundaries are then compiled into a single map of raw, irregularly spaced isobaths (Fig. 4, lower left).

Lake ice growth is simulated using the Liston and Hall (1995a, b) numerical model. The simulated ice-growth curve for winter 1991–92 (Fig. 5) originally appeared in Jeffries et al. (1996), which includes a detailed description of the numerical ice-growth model and its particular application in the Barrow region. In short, an energy balance model, driven by inputs of air temperature, wind speed and precipitation (in this case from the National Weather Service Station at Barrow), is coupled to lake mixing, snow, and lake ice submodels that force lake water temperatures, snow accumulation/metamorphism and lake ice growth. Daily ice thickness values are compiled into a simulated ice-growth curve, which must be for the winter corresponding to the sequence of SAR images being used to map lake bathymetry.

The raw isobaths are irregularly spaced, as image acquisition is temporally irregular and ice growth rates are nonlinear (Figs. 4 and 5). Thus, the final step in the procedure is to interpolate and filter between the raw isobaths to create a raw Digital Elevation Model (DEM), from which a final bathymetric chart of regularly spaced

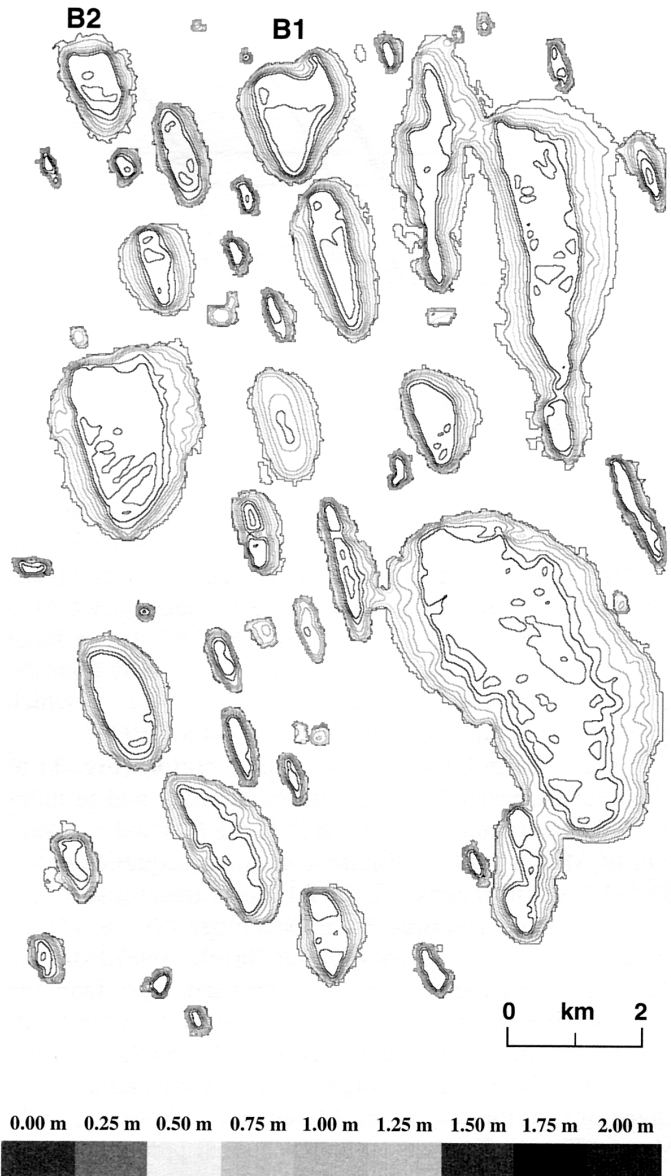


FIG. 6. Bathymetric charts derived using thresholding to identify the boundaries between floating and grounded ice for lakes in a 10 km × 15.6 km portion of the 'B' Lakes region.

(0.25 m) isobaths is extracted (Fig. 4, lower right). A 0.25 m isobath interval was chosen for the level of detail it provides on depth variability in often shallow waters. Jeffries et al. (1996) found that the entire surface area of 77% of the lakes near Barrow had frozen completely to the bottom by the end of winter, i.e., all those lakes had a maximum water depth less than the simulated maximum ice thickness of 2.21 m. In this case, an isobath interval of 0.5 m, for example, would greatly reduce the amount of bathymetric information about these lakes. Detailed bathymetric information is important for a number of reasons. For example, emergent aquatic plants in the shallow waters of these lakes are important conduits for gas exchange between the lake sediments and the atmosphere, but different species occupy different water depth zones

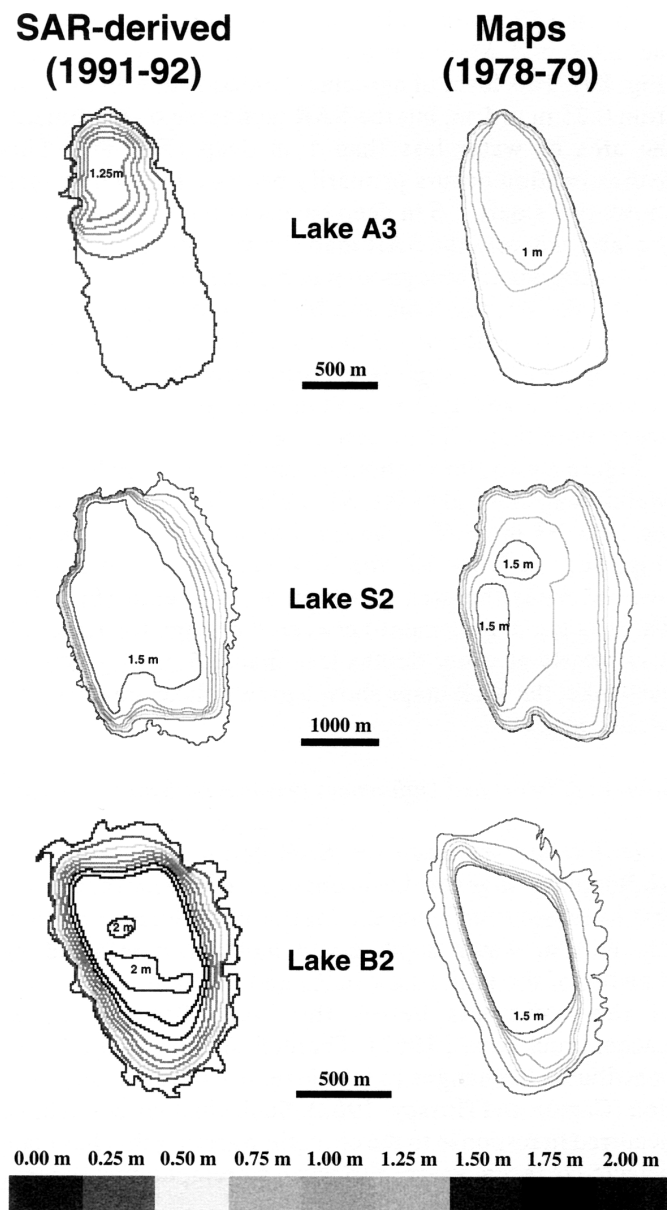


FIG. 7. Bathymetric maps for lakes A3, S2, and B1 derived using thresholding as the basis for the SAR mapping procedure (left) and those obtained from field measurements by Mellor (1982) in 1978–79 (right).

and exchange gases at different rates (e.g., Chanton et al., 1992). Since these gases include radiatively important greenhouse gases such as methane, a detailed knowledge of the bathymetry of the shallow waters would be important in the calculation and simulation of the gas fluxes and their contribution to regional methane budgets.

Because SAR data with clear boundaries between floating and grounded ice are not available until early December, when the ice is already 1 m thick (Fig. 5), there are no raw isobaths between 0 m and 1 m. Consequently, the final, equally spaced isobaths in these shallower waters are entirely the result of interpolation. This technique provides no bathymetric data for water less than 2 m deep, and no information on maximum water depth for lakes where the entire ice cover does not freeze completely to the

bottom. We do not interpolate beyond 2 m water depth because the simulated maximum ice thickness was 2.21 m in May 1992 (Fig. 5), i.e., lower than the next available final isobath (2.25 m). For lakes where the entire ice cover does freeze completely to the bottom, maximum water depth can be derived using either this technique or the one described by Jeffries et al. (1996).

The example presented here uses six SAR subscenes. Bathymetric maps were compiled using as few as two and as many as 13 SAR subscenes to determine the number required to obtain a satisfactory product. The first image and the last image of each set were always the earliest and latest available images of the sequence. A minimum of six images was found to be the threshold value. With fewer images, there were significant differences between the bathymetric maps, while increasing the number of images above the threshold did not yield a significant improvement.

The SAR technique can map a single lake or many lakes. We have illustrated the basic bathymetric mapping procedure using Lake B1 as an example. However, the procedure can be applied to larger areas containing multiple lakes, as shown in Figure 6, a set of bathymetric maps for the 'B' Lakes region identified in Figure 1.

#### COMPARISON OF SAR-DERIVED MAPS AND EXISTING MAPS

##### *Existing Bathymetric Maps*

We do not have our own measurements of lake depth with which to test the accuracy of the SAR technique for bottom mapping. For this we must rely on bathymetric maps compiled by Mellor (1982) at a few lakes in the 'A,' 'B,' and 'S' Lakes regions (Fig. 1). Mellor (1982) obtained water depth data during the summers of 1978 and 1979 using a 192 kHz sonar suspended between the floats of an airplane, which then taxied across each lake at a constant speed. Two depth profiles were acquired along transects across each lake, except for Lake B1, where three transects were used. Based on the shape of the lake boundary, Mellor (1982) interpolated water depth between transects to derive bathymetric maps with 0.5 m intervals.

To test the accuracy of our technique for bathymetric mapping using SAR data, we used the data obtained at six lakes by Mellor (1982). The analogue bathymetric maps for the lakes were digitized and interpolated to construct a Digital Elevation Model of each lake basin. Bathymetric maps with 0.25 m spacing consistent with that of the SAR-derived isobaths were then extracted from each DEM. The interpolation and isobath extraction procedures were the same as those used to derive isobaths from SAR data (see Appendix). For simplicity, we will refer to the 1978–79 maps as the Mellor maps. The comparison of the data is based on the surface area of water between 0 m and a particular contour. The 0 m contour is the lake margin and defines the total lake area.

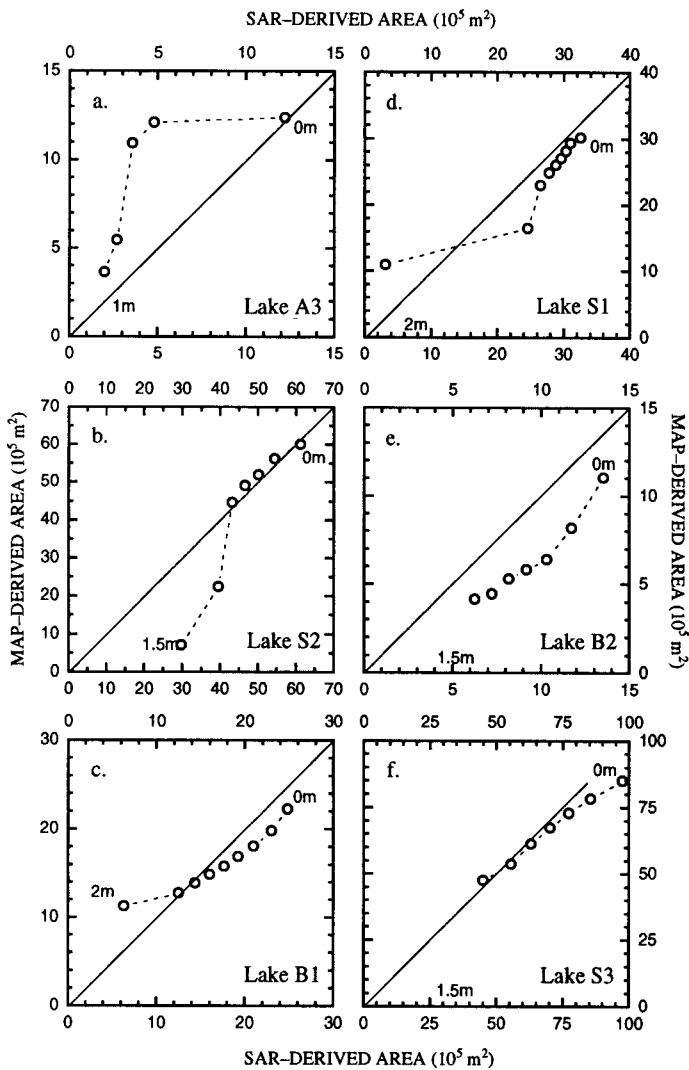


FIG. 8. Comparison of bathymetric data for six lakes obtained using the SAR mapping procedure and from the Mellor maps. The comparison is based on the surface area of water enclosed by the lake edge (0 m) and a particular isobath. Each data point represents an isobath, beginning at 0 m and then descending in 0.25 m increments to a maximum of 2 m. The thin, sloping line represents a 1:1 relationship between the SAR-derived area and the area obtained from the 1978–79 maps.

#### SAR-Derived Bathymetric Data versus Existing Bathymetry Data

The SAR-derived and Mellor maps for three lakes are shown in Figure 7. Qualitatively, the charts look reasonably similar in terms of their general shape and bottom topography. However, there are clearly some significant differences, and these are highlighted by the more quantitative comparison of the maps based on the surface area of water.

There is close agreement between the SAR and Mellor maps in terms of the area of Lake A3, i.e., the 0 m contour (Fig. 8a). However, the SAR technique grossly underestimates the area of water between 0.25 m and 0.75 m deep (Fig. 8a), primarily because the basin in the northern part of the lake is smaller in the SAR map than in the Mellor map (Fig. 7). Also, the SAR map of Lake A3 shows water that is less than 1 m deep, while the Mellor map does not (Fig. 7).

At Lake S2, there is also very good agreement between the SAR and Mellor maps in terms of the lake area (Fig. 8b). This level of agreement extends to water depths from 0.25 m to 1 m, but the SAR technique overestimates the area of water less than 1 m deep (Fig. 8b). This overestimation occurs primarily because the Mellor map shows two small, 1.5 m deep basins in the western part of the lake, whereas the SAR map shows a broad expanse of 1.5 m deep water throughout much of the lake area (Fig. 7).

At Lake B1, the SAR and Mellor maps agree particularly well at depths of 1.5 m and 1.75 m (Fig. 8c). Otherwise the SAR map slightly overestimates the area of water between 0 m and 1.25 m, and underestimates the area of water more than 1.75 m deep (Fig. 8c).

Figure 8 also shows comparisons between the SAR and Mellor maps for Lakes B2, S1, and S3. The comparison of the Lake S1 maps (Fig. 8d) is similar to that of Lake B1 (Fig. 8c). At Lake B2, the SAR technique consistently overestimates the area of water of any depth (Fig. 8e). There is good agreement between the maps for Lake S3, particularly at water depths less than 1.5 m (Fig. 8f). At each lake, the SAR maps show a greater lake area than the Mellor maps.

#### Sources of Error and Differences between Bathymetric Maps

Differences between the SAR-derived maps and the Mellor maps might be due to changes in lake morphometry that have occurred since the Mellor maps were compiled. Changes in water depth could have been affected by thawing of the talik (thaw bulb) and resultant subsidence of the sediments below the lake (Brewer, 1958; Lachenbruch et al., 1962). Thermal erosion of the banks contributes to changes in lake size, orientation, and location (Carson and Hussey, 1962). Such changes could have occurred in response to the climatic warming that has been detected in recent years in Alaskan air temperature records (Chapman and Walsh, 1993).

The climate of the North Slope is not uniform. Zhang et al. (1996) have reported that the relatively warm coastal climate is due to a maritime effect, and that its influence decreases with distance from shore. Consequently, a colder, more continental climate prevails in the southern regions of the North Slope. The simulated ice-growth curve (Fig. 4) perhaps best represents the Barrow region, and errors in assignment of water depths to the raw isobaths occur when the same curve is applied to lakes outside the coastal region. The use of the Barrow ice-growth curve could lead to underestimation of the water depth in regions where a colder winter climate promotes thicker ice growth.

The accuracy of the water depths assigned to the raw isobaths depends on the accuracy of the simulated ice-growth curve. In this case, we are confident of its accuracy because the model was run in “data assimilation” mode, which uses field measurements to constrain the simulation (Jeffries et al., 1996). On the other hand, the SAR mapping technique does not create raw isobaths between 0 m and

1 m, and it relies entirely on interpolation to generate the final isobaths between those depths. This fact might account for the tendency of the SAR mapping technique to overestimate the depth of the shallower waters (Fig. 8). Regardless of the agreement between the SAR and Mellor maps, the SAR maps are probably most accurate at depths between 1 m and 2 m.

The SAR technique relies on the detection of the boundary between floating and grounded ice. Thus a small error in water depth estimation might arise because, from the moment the ice comes into contact with the bottom sediments, some time must elapse before those sediments freeze and dry sufficiently for the SAR signal to pass through the ice/sediment interface. During that time, the floating ice continues to grow. Consequently, the SAR technique will overestimate the water depth because the growing ice in fact came into contact with the sediment earlier than the time a particular SAR image was acquired and at a shallower water depth.

The SAR maps have been generated by an entirely digital technique. To assess their accuracy, we compared them with a digital product generated from the original analogue Mellor maps. The analogue-to-digital conversion is likely to be a source of inaccuracy. Furthermore, there are likely to be inaccuracies in the original analogue maps. Sampling along only two or three transects at a lake (Mellor, 1982) would miss details of the bottom topography, and creating spatially continuous isobaths by interpolation between those transects would compound the error. This conversion is therefore less accurate than the SAR technique, which uses interpolation only after spatially continuous raw isobaths have been determined by discriminating between the floating and grounded ice.

## SUMMARY AND CONCLUSION

We have described a digital technique that combines SAR remote sensing and a simulated ice-growth curve for bathymetric mapping of the shallow waters ( $\leq 2$  m) of tundra lakes. The basis of the technique is to map the changing boundary between floating ice and grounded ice in a sequence of wintertime SAR images, assign an ice thickness to each boundary from the simulated ice-growth curve for that particular winter, and interpolate between the raw isobaths to create a bathymetric chart with equally spaced isobaths. The SAR-derived bathymetric maps have been compared with existing bathymetric maps for the few lakes for which the latter are available. There is modest agreement between the SAR-derived and existing bathymetric maps based on comparisons of surface water area enclosed by the lake edge and a particular isobath. Differences between the SAR maps and the original maps are probably unavoidable because they differ in production method and original data format.

Our technique provides bathymetric data only for those waters that are shallower than the maximum ice thickness,

thus leaving large areas of some lakes with no water depth information. Nevertheless, we believe that the basic concept of using SAR and simulated ice-growth curves for bathymetric mapping is sound. Implementing this technique for routine, inexpensive, and accurate mapping could greatly increase the amount and spatial coverage of shallow water depth data in thaw lakes on the North Slope and elsewhere, e.g., in East Siberia, where similar lakes occur (Jeffries et al., 1996: Fig. 7). This mapping technique would benefit from verification based on new maps derived from accurate field measurements at a selection of lakes with different morphological characteristics. Accurate field-based and SAR-derived maps would provide an important baseline against which to judge future changes in lake size, shape, bottom topography, and location. Such information would be valuable in view of the sensitivity of the Arctic climate and its potential impact on the lake-dominated landscape of the North Slope and elsewhere.

The strength of the SAR mapping technique lies in the semiautomated generation of continuous raw isobaths from a relatively small number of SAR scenes. The assignment of a depth to those isobaths relies on the accurate simulation of lake ice growth. If this technique were to be applied to map lake bathymetry in different areas of the North Slope, or across the entire region, a number of simulated ice-growth curves that reflect regional climate variability would be preferred. Thresholding or classification (see Appendix) can be used equally well to define the lake margin, delineate the boundary between the floating ice and grounded ice, and derive satisfactory bathymetric data. Since thresholding is a simpler, computationally more efficient technique than classification, it would be preferred for mapping a large number of lakes in geographically large regions such as the North Slope and Siberia.

## ACKNOWLEDGEMENTS

This work was supported by NASA Polar Program grants NAGW-4966 and NAG5-4170. We thank Shusun Li, Kim Morris, Rainer Newberry, and Buck Sharpton for their comments on early versions of this paper, and the three reviewers for their constructive suggestions for improvements.

## APPENDIX: Semiautomated SAR Image Processing and Data Extraction for Mapping Thaw Lake Bathymetry

### *Generating the Lake Mask*

A lake mask, i.e., the lake boundary, is generated by binary summation of a mask corresponding to the boundary between the grounded ice and the tundra, and a mask corresponding to the boundary between the grounded and floating ice (Fig. A1). Without binary summation, erroneous lake masks would be generated in cases where floating ice is in direct contact with the tundra.

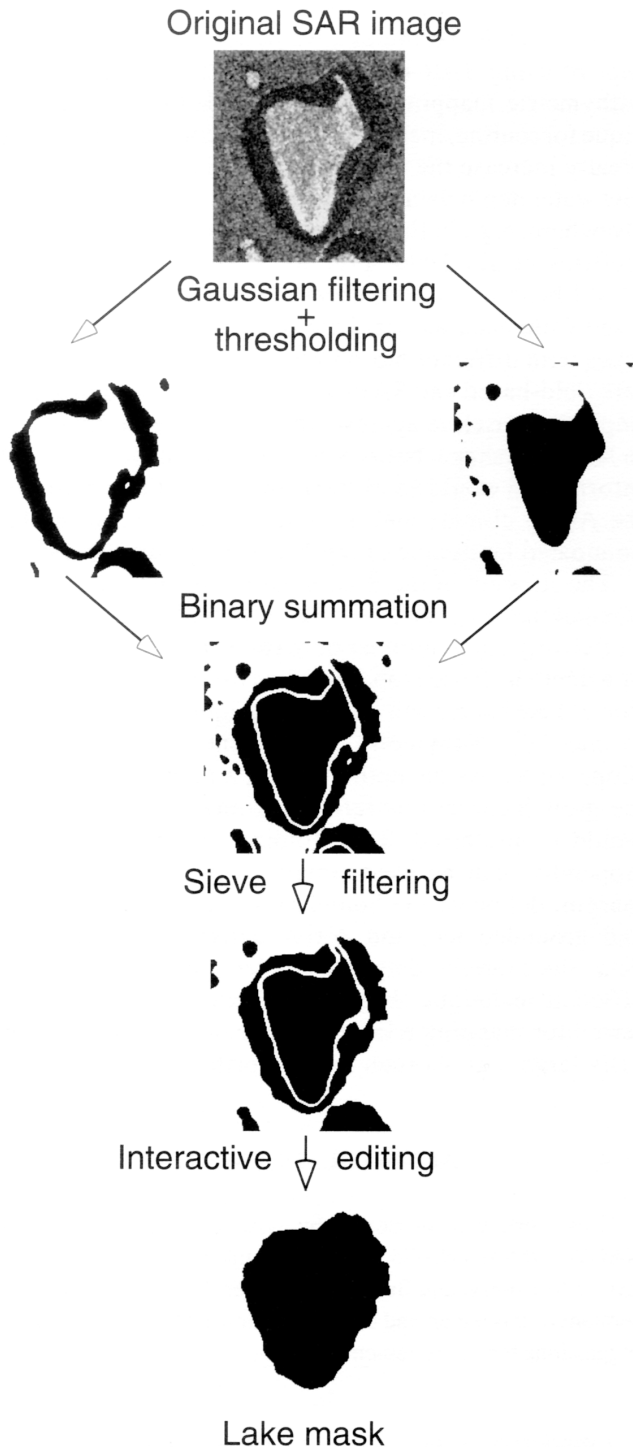


FIG. A1. Sequence of data transformations used to derive a lake mask from an SAR image (top) that shows floating ice (bright tone), grounded ice (dark tone), and tundra (intermediate grey tone around the periphery of the box).

To determine threshold values for masking the floating ice, we used a backscatter time series compiled for winter 1991–92 using sequential ERS-1 SAR imagery (Jeffries et al., 1994; Morris et al., 1995). The threshold values for the grounded ice ( $\sigma_{GI}^T$ ) and floating ice ( $\sigma_{FI}^T$ ) are calculated from observed differences in backscatter between grounded ice ( $\sigma_{GI}^o$ ), floating ice ( $\sigma_{FI}^o$ ), and frozen tundra ( $\sigma_{FT}^o$ ),

where  $\sigma_{GI}^o < \sigma_{FT}^o < \sigma_{FI}^o$ . These values are spatially averaged backscatter coefficients of grounded ice, frozen tundra and floating ice, respectively. Specifically,  $\sigma_{GI}^T = (\sigma_{GI}^o + \sigma_{FT}^o) / 2$  and  $\sigma_{FI}^T = (\sigma_{FT}^o + \sigma_{FI}^o) / 2$ .

The last image from the source sequence is used to construct the lake mask, since it is characterized by nearly maximum ice thickness and consequently by maximum backscatter contrast between the areas of floating ice, grounded ice, and frozen tundra. The quantities  $\sigma_{GI}^o$ ,  $\sigma_{FT}^o$ , and  $\sigma_{FI}^o$  are estimated from the source SAR image or derived from time-dependent empirical backscatter curves (Jeffries et al., 1994; Morris et al., 1995).

To eliminate residual noise and enhance the resulting mask, a sieve filter and an interactive bit mask editor are used. The sieve filter is a morphological operator that removes all polygons smaller than a user-specified size. Polygons smaller than the threshold are merged with their largest neighbour. Interactive editing is used to fill unavoidable gaps between the two masks generated by thresholding with  $\sigma_{GI}^T$  and  $\sigma_{FI}^T$ .

#### *Filtering the SAR Image*

To improve the efficiency of the discrimination between floating ice, grounded ice, and frozen tundra, the SAR images are preprocessed by a low-pass filter (Fig. A2). We used a linear filter with Gaussian kernel for two reasons. First, it is rotationally symmetric, so the amount of smoothing is the same in all directions. Second, compared to other linear filters, it provides the best compromise between noise immunity and localization of the high-contrast edges (Schunk, 1992; Schowengerdt, 1997:273–276).

#### *Constructing and Enhancing the Floating Ice Mask*

Two standard techniques are available to construct the mask representing the area of floating ice: thresholding and classification (Fig. A2). Thresholding is a simpler, computationally more efficient technique. Classification based on a maximum likelihood criterion is statistically better justified, but it is computationally more expensive. It also requires the user to define training sites for calculating backscatter signatures of the floating ice. In any event, a comparison of the area of water enclosed by the lake margin and a given contour in maps derived by thresholding and by classification (Fig. A3) indicates that the differences between the two techniques are minimal.

To determine the threshold value for the floating ice, the basic procedure applies an approach similar to that used for generating the lake mask. Since the area of frozen tundra has been masked out in the previous step, the floating ice threshold value is calculated according to  $\sigma_{FI}^T = (\sigma_{GI}^o + \sigma_{FI}^o) / 2$ . The mask resulting from either thresholding or classification is enhanced with a sieve filter (Fig. A2). The filter is applied twice: the first time to

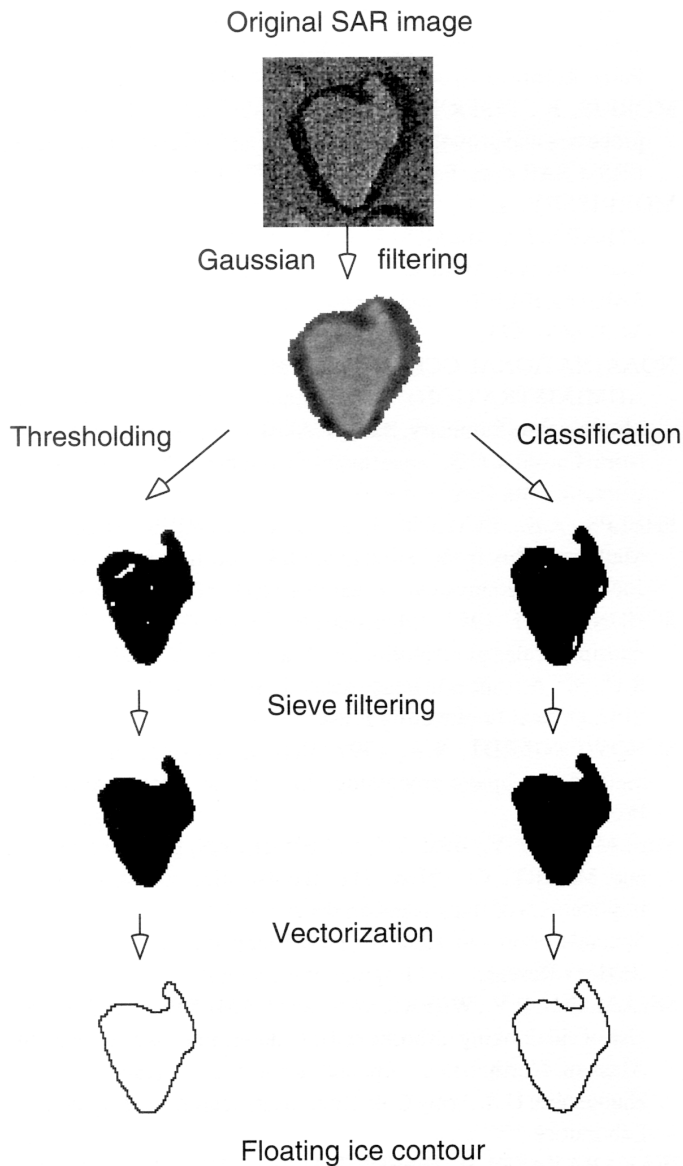


FIG. A2. Sequence of data transformations used to map the boundaries between the floating ice and grounded ice in SAR images according to thresholding (left) or classification (right) after the SAR image has been subject to Gaussian filtering (top).

eliminate noise polygons and the second time to patch voids in the mask.

#### *Extraction of Isobaths, and Derivation and Smoothing of a Digital Elevation Model*

The boundary between floating ice and grounded ice is extracted from the mask generated in the previous step with a standard vectorizing technique (Fig. A2). Once the boundary between the floating ice and grounded ice has been derived according to the steps illustrated in Figure A2, an ice thickness is assigned to that contour/isobath, as previously described in the text. Once the raw isobaths have been generated, interpolation between the raw isobaths is applied to generate a Digital Elevation Model (DEM) of

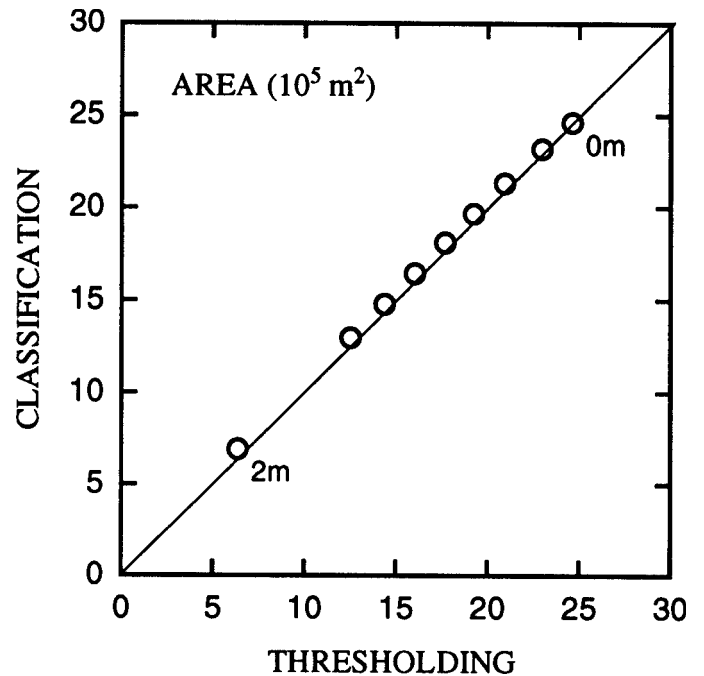


FIG. A3. Comparison of the thresholding and classification techniques used to derive bathymetric charts from SAR images of Lake B1. The comparison is based on the surface area of water enclosed by 0 m (lake edge) and a particular isobath. The thin, sloping line represents a 1:1 relationship between thresholding and classification. The maximum difference is 8%.

the lake basin. The interpolation algorithm is based on a Morphology-Dependent Interpolation Procedure (MDIP) (Carrara, 1988). The procedure searches in eight directions for the location of the two nearest contours, and it interpolates between those contours depending on the morphological type of the pixel of interest (slope, depression, or peak). The algorithm fails if the floating ice contours extracted from the SAR images intersect each other. This happens if the slope of the lake bed is too steep and the local backscatter variability is relatively high. The lake basin DEM is smoothed using a 3 pixel by 3 pixel ( $37.5 \text{ m} \times 37.5 \text{ m}$ ) Gaussian filter that is sufficient to hide any artifacts resulting from the interpolation procedure. A standard contour linking procedure is applied to extract regularly spaced isobaths (0.25 m interval) from the DEM.

#### REFERENCES

- BREWER, M.C. 1958. The thermal regime of an Arctic lake. *Transactions of the American Geophysical Union* 39(2): 278–284.
- CARRARA, A. 1988. Drainage and divide networks derived from high-fidelity digital terrain models. In: *NATO Advanced Study Institute on Statistical Treatments for Estimation of Mineral and Energy Resources*, 22 June–4 July 1986, Il Ciocco (Lucca), Italy. NATO ASI Series C, Mathematical and Physical Sciences, 223. Norwell, Boston, Massachusetts: Kluwer Academic. 581–597.

- CARSON, C.E., and HUSSEY, K.E. 1962. The oriented lakes of Arctic Alaska. *Journal of Geology* 70(4):417–439.
- CHANTON, J.P., MARTENS, C.S., KELLEY, C.A., CRILL, P.M., and SHOWERS, W.J. 1992. Methane transport mechanisms and isotope fractionation in emergent macrophytes of an Alaskan tundra lake. *Journal of Geophysical Research* 97(D15):16,681–16,688.
- CHAPMAN, W.L., and WALSH, J.E. 1993. Recent variations of sea ice and air temperatures in high latitudes. *Bulletin of the American Meteorological Society* 74(1):33–47.
- DEAN, K.G., and MORRISSEY, L.A. 1988. Detection and identification of Arctic landforms: An assessment of remotely sensed data. *Photogrammetric Engineering and Remote Sensing* 54(3):363–371.
- ELACHI, C., BRYAN, M.L., and WEEKS, W.F. 1976. Imaging radar observations of frozen Arctic lakes. *Remote Sensing of Environment* 5(3):169–175.
- HALLIKAINEN, M., and WINEBRENNER, D.P. 1992. The physical basis for remote sensing. In: Carsey, F.D., ed. *Microwave remote sensing of sea ice*. Geophysical Monograph 68. Washington, D.C.: American Geophysical Union. 29–46.
- JEFFRIES, M.O., MORRIS, K., WEEKS, W.F., and WAKABAYASHI, H. 1994. Structural and stratigraphic features and ERS-1 synthetic aperture radar backscatter characteristics of ice growing on shallow lakes in NW Alaska, winter 1991–1992. *Journal of Geophysical Research* 99(C11):22,459–22,471.
- JEFFRIES, M.O., MORRIS, K., and LISTON, G.E. 1996. A method to determine lake depth and water availability on the North Slope of Alaska with spaceborne imaging radar and numerical ice growth modelling. *Arctic* 49(4):367–374.
- JEFFRIES, M.O., ZHANG, T., FREY, K., and KOZLENKO, N. 1999. Estimating late winter heat flow to the atmosphere from the lake-dominated Alaskan North Slope. *Journal of Glaciology* 45(150):315–324.
- LACHENBRUCH, A.H., BREWER, M.C., GREENE, G.W., and MARSHALL, B.V. 1962. Temperatures in permafrost. *Temperature - Its Measurement and Control in Science and Industry* 3(1):791–803.
- LECONTE, R., and KLASSEN, P.D. 1991. Lake and river ice investigations in northern Manitoba using airborne SAR imagery. *Arctic* 44(Supp. 1):153–163.
- LISTON, G.E., and HALL, D.K. 1995a. An energy balance model of lake ice evolution. *Journal of Glaciology* 41(138):373–382.
- . 1995b. Sensitivity of lake freeze-up and break-up to climate change: A physically based modelling approach. *Annals of Glaciology* 21:387–393.
- LYTLE, V.I., JEZEK, K.C., GOGINENI, S.P., and HOSSEINMOSTAFA, A.R. 1996. Field observations of microwave backscatter from Weddell Sea ice. *International Journal of Remote Sensing* 17(1):167–180.
- MELLOR, J.C. 1982. Bathymetry of Alaskan Arctic lakes: A key to resource inventory with remote sensing methods. Ph.D. thesis, Institute of Marine Science, University of Alaska.
- . 1994. ERS-1 SAR use to determine lake depths in arctic and subarctic regions. In: *Proceedings of the Second ERS-1 Symposium—Space at the Service of our Environment*, 11–14 October 1993, Hamburg, Germany. Special Publication SP-361. Paris: European Space Agency. 1141–1146.
- MORRIS, K., JEFFRIES, M.O., and WEEKS, W.F. 1995. Ice processes and growth history on arctic and subarctic lakes using ERS-1 SAR data. *Polar Record* 31(177):115–128.
- MORRISSEY, L.A., DURDEN, S.L., LIVINGSTON, G.P., STEARN, J.A., and GUILD, L.S. 1996. Differentiating methane source areas in Arctic environments with multitemporal ERS-1 SAR data. *IEEE Transactions on Geoscience and Remote Sensing* 34(3):667–673.
- NOAA (NATIONAL OCEANOGRAPHIC AND ATMOSPHERIC ADMINISTRATION). 1992. Local Climatological Data, Monthly Data Summary, Barrow, Alaska, March 1992. Asheville, North Carolina: U.S. Department of Commerce, NOAA, National Climatic Data Center. 4 p.
- PHELPS, A.R., PETERSON, K., and JEFFRIES, M.O. 1998. Methane efflux from high latitude lakes during spring ice-melt. *Journal of Geophysical Research* 103(D2):29,029–29,036.
- SCHUNK, B.G. 1992. Edge detection with Gaussian filters at multiple scales of resolution. In: Mahdavi, Y., and Gonzalez, R.C., eds. *Advances in image analysis*. Bellingham, Washington: SPIE Optical Engineering Press. 75–105.
- SCHOWENGERDT, R.A. 1997. *Remote sensing, models and methods for image processing*. 2nd ed. San Diego: Academic Press. 522 p.
- SELLMANN, P.V., BROWN, J., LEWELLEN, R.I., McKIM, H., and MERRY, C. 1975a. The classification and geomorphic implications of thaw lakes on the Arctic Coastal Plain, Alaska. Special Report 344. Hanover, New Hampshire: U.S. Army Cold Regions Research and Engineering Laboratory.
- SELLMANN, P.V., WEEKS, W.F., and CAMPBELL, W.J. 1975b. Use of sidelooking airborne radar to determine lake depth on the Alaskan North Slope. Special Report 230. Hanover, New Hampshire: U.S. Army Cold Regions Research and Engineering Laboratory.
- WAKABAYASHI, H., JEFFRIES, M.O., and WEEKS, W.F. 1994. C band backscatter variation and modelling for lake ice in northern Alaska (in Japanese with English abstract). *Journal of the Japanese Remote Sensing Society* 14(3):18–27.
- WEEKS, W.F., SELLMANN, P., and CAMPBELL, W.J. 1977. Interesting features of radar imagery of ice-covered North Slope lakes. *Journal of Glaciology* 18(78):129–136.
- WEEKS, W.F., FOUNTAIN, A.G., BRYAN, M.L., and ELACHI, C. 1978. Differences in radar return from ice-covered North Slope lakes. *Journal of Geophysical Research* 83(C8):4069–4073.
- WEEKS, W.F., GOW, A.J., and SCHERTLER, R.J. 1981. Ground-truth observations of ice-covered North Slope lakes imaged by radar. Special Report 81-19. Hanover, New Hampshire: U.S. Army Cold Regions Research and Engineering Laboratory.
- ZHANG, T., OSTERKAMP, T.E., and STAMNES, K. 1996. Some characteristics of the climate in northern Alaska, U.S.A. *Arctic and Alpine Research* 28(4):509–518.